

# Seismic evaluation of an eight story building with self-centering steel moment resisting frames and flange friction devices.



**P. Rojas**

*Escuela Superior Politécnica del Litoral, Ecuador  
Universidad Católica de Santiago de Guayaquil, Ecuador*

**D.C. Suárez**

*Escuela Superior Politécnica del Litoral, Ecuador*

**J. M. Ricles & R. Sause**

*Lehigh University, United States*

## SUMMARY:

During the last decade, extensive research has been carried out on self-centering (SC) steel moment resisting frames (MRFs). Previous research of SC-MRFs with post-tensioned flange friction devices (PT-FFD) beam-to-column connections has been carried out using a four-30 feet bays six story frame. Therefore, there is a need to investigate this system for taller framed buildings with different length and number of bays. Thus, the focus of this research is to evaluate the seismic performance of a three-25 feet bays eight story SC steel MRF building with PT-FFD connections. These SC systems use gap-opening behavior at selected joints between main structural members, along with associated friction devices, to provide nonlinear softening behavior, ductility, and energy dissipation without significant inelastic deformation and related damage to the main structural members. Elastic restoring forces provided by post-tensioning (PT) at these joints return the structure to its original position, eliminating residual drift. Beam flanges friction devices (FFD) are included at each PT connection as energy dissipation elements.

*Keywords: Seismic Evaluation; self-centering; moment resisting frame building; friction devices; connections*

## 1. INTRODUCTION

Extensive research has been carried out on self-centering (SC) steel moment resisting frames (MRFs) in several countries as an alternative to traditional construction of steel MRFs in seismic areas. One type of these systems combines post-tensioned beam-to-column connections with passive dampers. Passive dampers are usually hysteretic dampers which dissipate energy either through metal yielding or friction sliding mechanisms. This paper focuses in SC-MRFs that use post-tensioned beam-to-column connections that include passive frictional dampers. The dampers are located at the upper and lower flanges of the beams. For this reason, the beam-to-column connections are referred in this paper as the *post-tensioned flange friction devices* (PT-FFD) connection.

The analytical and experimental research on SC-MRFs with PT beam-to-column connections and passive frictional dampers (Rojas 2003, Caballero 2005, Wolski et al. 2006, Iyama et al. 2008, and Lin et al. 2008) subjected to severe ground motions show that these systems exhibit adequate strength, stiffness, ductility, and especially self centering capabilities. The systems have essentially no structural damage and thus, the residual drift is almost negligible if significant residual deformation does not occur at the base of the ground floor columns. These characteristics are desirable especially in those communities where the buildings are expected to resist moderate and severe earthquake ground motions, and their aftershocks, with no disturbance to business operations and avoiding the need of long downtime periods and the associated repair costs.

Previous research of SC-MRFs with post-tensioned flange friction devices (PT-FFD) beam-to-column connections has been carried using a four-30 feet bays six story frame using the design methodology presented by Rojas (2003). However, there is a need to investigate the seismic performance of this

system for taller framed buildings with different length and number of bays. Therefore, the focus of this research is to evaluate the seismic performance of a three-25 feet bays eight story SC steel MRF building with PT-FFD beam-to-column connections. The seismic evaluation is discussed presenting the results of nonlinear static pushover and dynamic analyses. The dynamic analyses were carried out at the Design Basis Earthquake (DBE) and Maximum Considered Earthquake (MCE) levels using a set of four ground motions.

**2. DESCRIPTION OF A SC-MRF WITH PT-FFD CONNECTIONS**

**2.1. System and Connection Details**

A SC-MRF with PT-FFD connections consists of beams, columns, PT high strength strands and passive friction dampers as shown in Figure 1. The PT strands run parallel to the beams across multiple bays through the columns, and are anchored outside the connection region as seen in Figure 2. The high strength steel strands are post-tensioned after the friction devices are installed. Due to the initial post-tensioning force applied to the strands, the beam flanges are compressed against the column flanges. Reinforcing plates, welded on the outside faces of the beam flanges, are needed to avoid excessive compression yielding in the beam flanges. Shim plates are placed between the column flange and the beam flanges so that only the beam flanges and reinforcing plates are in contact with the column. This enables good contact to be maintained between the beam flanges and column face, while protecting the beam web from yielding under bearing.

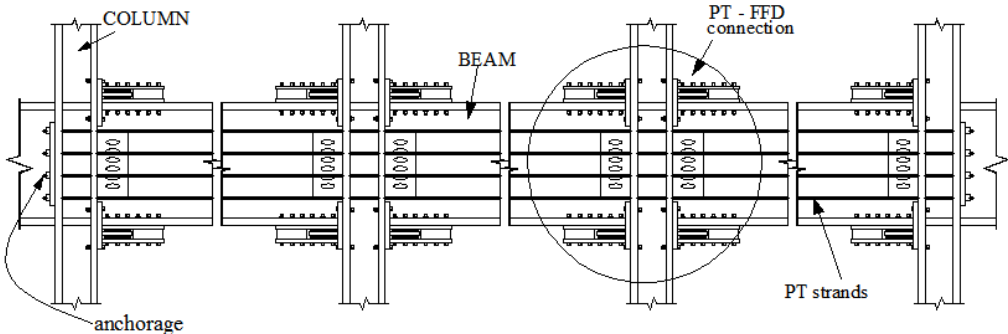


**Figure 1.** Schematic elevation of one floor of a SC-MRF with PT-FFD connections

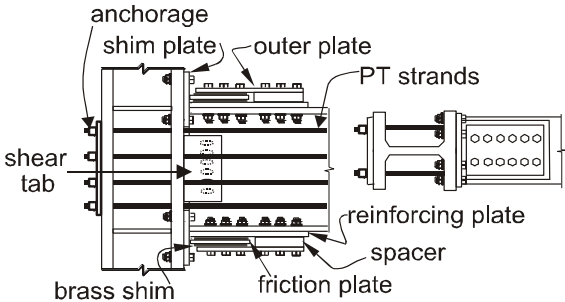


**Figure 2.** Connection details

The friction devices located at the beam flanges consist of a friction plate sandwiched by two brass shim plates that are inserted between the beam flange reinforcing plate and an outer plate. All plates are bolted to the beam flanges. Long slotted holes are drilled on the friction plate to accommodate the travel of the friction bolts during gap opening and closing of the connections that is discussed later. The shim plate serves as a tee flange that the friction plate is attached to. Friction is generated when the beam flanges and outer plate slide against the stationary friction plate when the beam rotates about the center of rotation (COR) situated at the mid-depth of the reinforcing plates (see Figure 3 insert). The brass shim plates are used to produce a stable friction force and to control the energy capability of

the PT-FFD connection. A shear tab with slotted holes is bolted to the beam web and welded to the column flange to transmit the shear forces.

## 2.2. Moment-relative rotation behavior

The moment-relative rotation ( $M-\theta_r$ ) behavior for a PT-FFD connection when subjected to cyclic loading is shown in the schematic given in Figure 3. The behavior is characterized by a gap opening and closing at the beam-column interface. The total moment resistance of the connection is provided by the moment due to the initial post-tensioning force in the strands, friction force, and an additional force developed due to elongation of the strands. For simplicity, the post-tensioned forces are assumed to be acting at the centroidal axis of the beam while the friction forces are assumed to be acting at the mid-depth of top and bottom friction plates.

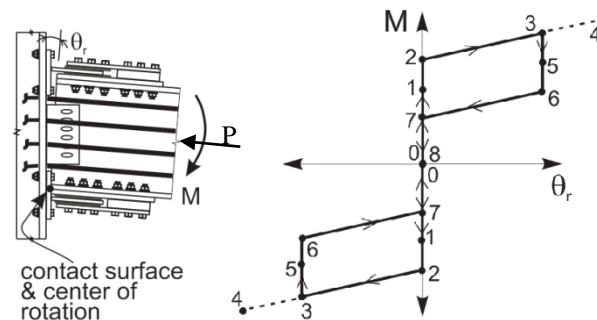


**Figure 3.** Moment-relative rotation behavior

Under applied moment, the connection initially behaves as a fully restrained (FR) connection, where the initial stiffness is similar to that of a fully restrained welded moment connection when  $\theta_r$  is equal to zero (events 0 to 2 in Fig. 3). Once the magnitude of the applied moment reaches the moment resistance due to the initial post-tensioning force in the strands, decompression of the beam from the column face occurs. The moment at which this occurs (event 1) is called the decompression moment. The applied moment continues to increase between events 1 and 2 as the rotation of the beam is restrained by the resistance of the friction component. At event 1 the friction force is minimal and increases gradually up to its maximum value at point 2, which is the point of incipient rotation. The maximum value of the friction force is computed using classical friction Coulomb's theory.

The stiffness of the connection after gap opening is associated with the elastic axial stiffness of the post-tensioned strands. With continued loading, the strands elongate, producing an additional force, which contribute to resist the total applied moment. Yielding of the strands eventually may occur at event 4. Upon unloading (event 3),  $\theta_r$  remains constant. At event 5, the friction force is zero. Between events 5 and 6 the friction force changes direction and starts increasing until reaching its maximum value at event 6. Between events 6 and 7, the beam rotates until the beam top flange is back in contact with the shim plate, but not compressed. Between events 7 and 8 the value of the friction force decreases with the beam being compressed against the shim plates and  $M$  equal to zero at event 8. A complete reversal in the applied moment will result in a similar connection behavior occurring in the opposite direction of loading, as shown in Fig. 3.

As long as the strands remain elastic, and there is no significant beam yielding, the post-tensioning force is preserved and the connection will self-center upon unloading (i.e.,  $\theta_r$  returns to zero rotation upon removal of the connection moment and the structure returns to its pre-earthquake position). The energy dissipation capacity of the connection is related to the force developed between the friction surfaces.

### 2. 3. Moment Capacity of the Connection

After gap opening, the moment capacity  $M$  of the connection is controlled by the beam axial force and the friction force developed at the FFD as follows:

$$M = d_1 F_f + P d_2 \quad (2.1)$$

where  $F_f$  is the maximum friction force assumed to be acting at the mid-depth of the friction plate attached to the beam tension flange,  $P$  is the beam axial force, and  $d_1$  and  $d_2$  are the distances from the line of actions of  $F_f$  and  $P$  to the center of rotation (COR) located at the mid-depth of the reinforcing plates, respectively. The values of  $F_f$ , and  $P$  are estimated using the following equations:

$$F_f = 2\mu N \quad (2.2)$$

$$P = T + F_{fd} \quad (2.3)$$

where  $\mu$  is the friction coefficient,  $N$  is the normal force generated by the pretensioned bolts placed through the slotted holes of the friction plates between the tribo surfaces, and the factor 2 is due to the presence of two sliding surfaces on each friction plate. In Equation (2.3),  $T$  is the post-tensioning strand force and  $F_{fd}$  is an additional beam axial force, produced by the interaction of the SC-MRF frame with the floor diaphragm (further details about this interaction can be found in Rojas 2003). The value of  $T$  is given by Equation (2.4) as follows:

$$T = T_o + 2d_2 \left( \frac{k_b k_s}{k_b + k_s} \right) \theta_r \quad (2.4)$$

where  $T_o$  is the sum of the initial post-tensioning force in all strands,  $k_s$  and  $k_b$  are the total strand stiffness and beam axial stiffness, respectively, and  $d_2$  and  $\theta_r$  were defined above.

### 3. PERFORMANCE BASED DESIGN PROCEDURE

A performance based design (PBD) procedure is used for the SC-MRF studied in this research. The PBD considers two levels of expected earthquake ground motions related to two seismic building performance levels. The two expected ground motion levels defined in FEMA 450 (FEMA 2003) are: (1) the design basis earthquake (DBE); and (2) the maximum considered earthquake (MCE). The MCE has a 2% probability of being exceeded in 50 years while the DBE is defined as 2/3 the intensity of the MCE, with an approximate 10% probability of being exceeded in 50 years. The two seismic performance levels are: (1) the “immediate occupancy” performance level, which describes a post-earthquake damage state in which only limited structural and nonstructural damage has occurred; and (2) the “collapse prevention” performance level, which describes a post-earthquake damage state in which the building is on the verge of partial or total collapse.

The proposed design approach developed for SC-MRFs with PT-FFD connections has two performance objectives: (1) to achieve the immediate occupancy level under DBE ground motions; and (2) to achieve the collapse prevention level under MCE ground motions. Under DBE ground motions, the structural components of the system should not develop inelastic behavior, except for minimal yielding in the beam flanges at the end of the reinforcing plates. As a result, the building is ready to be reoccupied after the DBE ground motions. The PT strands and the flange friction devices are designed to remain elastic under MCE ground motions. Some inelastic behavior is expected in the panel zones, beams, and columns, with the onset of local buckling occurring in a few of the beams. With an appreciable amount of local beam buckling, a loss of post-tensioning would occur leading to a degradation in frame capacity. Thus, under MCE ground motions, the frame is expected to lose some

of its self-centering capacity, but not collapse.

#### 4. DESCRIPTION AND DESIGN OF PROTOTYPE SC-MRF

As mentioned above, Rojas (2003) studied the seismic performance of a 6-story and 4 bay perimeter SC-MRF where each bay had a length of 9150 mm (30'). This frame was designed using the equivalent lateral force procedure (ELFP) of IBC 2000. As a continuation of that work, in this study an 8-story, 3-bay perimeter SC-MRF where each bay has a length of 7622 mm (25') was designed as a MRF with PT-FFD beam-to-column connections. The objective of this study is to evaluate the seismic performance of these systems for taller framed buildings with length and number of bays different than those used in Rojas (2003). The frame was designed using the ASCE/SEI 7-10 seismic provisions. The following assumptions were made: (1) Modal response spectrum analysis for special MRFs was applicable according to Table 12.6-1 of ASCE/SEI 7-10 instead of the ELFP used by Rojas (2003); (2) the structure is an office building located on stiff soil in the Los Angeles area; (3) the design accelerations were determined using the deterministic limit of the ASCE/SEI 7-10 site-specific procedure; (4) A992 steel sections were used; and (5) an elastic structural model of the building was developed with the aid of the SAP 2000 software. The plan of the building, including the layout of the gravity and the SC-MRFs, is shown in Figure 4(a). An elevation view of the prototype frame, including the member sizes for the frame, is shown in Figure 4(b).

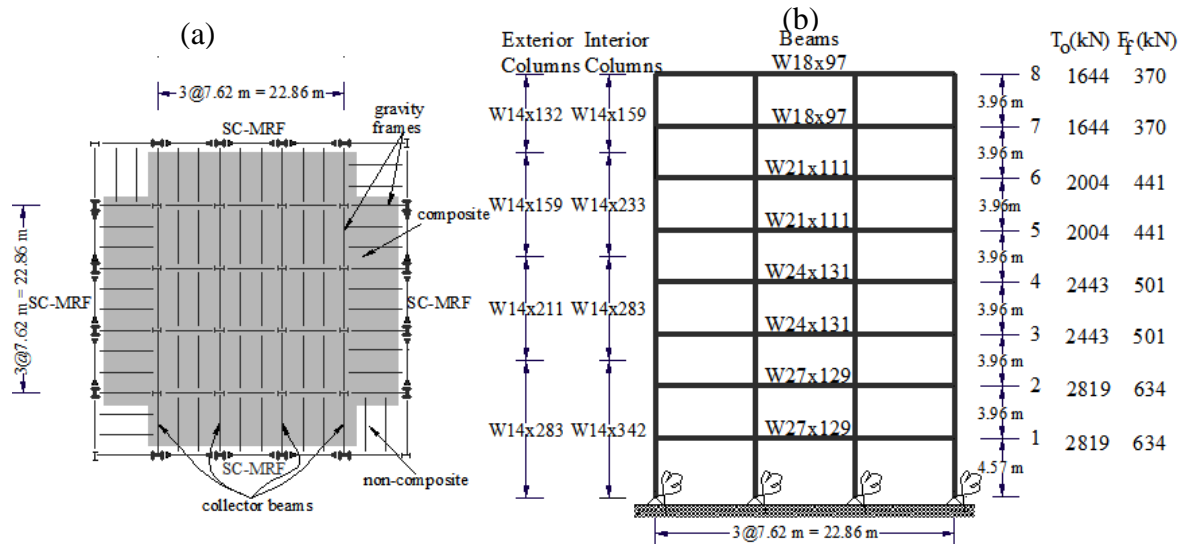


Figure 4. Prototype building

Applying the recommendations given by Rojas (2003), an elastic analysis of the building was performed using a response modification coefficient (R) and a deflection amplification factor ( $C_d$ ) of 8 and 5.5, respectively. The design base shear was  $0.037W$ . The forces and the drifts were scaled according to section 12.9 of ASCE/SEI 7-10. The resulting interstory drifts in the building ranged between 0.62% and 1.30% from the upper to the lower stories, respectively.

Following the design methodology presented in Rojas (2003), the design of the PT-FFD connections resulted in a connection average flexural capacity of  $0.96 M_{p,n}$  (where  $M_{p,n}$  is the nominal plastic capacity of the beam) throughout of the frame at the connection deformation  $\theta_{r,DBE}$  of 0.027 rad. The reinforcing plates were required to be 1524 mm (60 pulgadas) long with thicknesses of 25 mm and 19 mm at the lower and upper stories, respectively. Doubler plates were only required at almost every interior panel zone. The initial post-tensioning ( $T_o$ ) and the maximum friction forces ( $F_f$ ) provided at the SC-MRF are summarized in Figure 4(b). The values for  $T_o$  range from 45% (first floor) to 35% (roof) of the strand tensile force capacity  $T_u$ , with the strand yield force equal to about  $0.90 T_u$ . The values for  $F_f$  were determined using a friction coefficient  $\mu$  of 0.40, resulting in a reasonable number

of bolts through the friction plates.

## 5. ANALYTICAL MODELING OF SC-MRF WITH PT-FFD CONNECTIONS

An analytical model of a PT-FFD connection and the associated beams and columns was developed using the DRAIN-2DX computer program (Prakash *et al.* 1993, Herrera *et al.* 2001) as described in Rojas (2003). Figure 5 shows the analytical model. Beams and columns are modeled using fiber elements that are divided into a number of segments which are comprised of several fibers. A material stress-strain relationship, a cross sectional area, and a distance from the longitudinal reference axis of the member characterize each fiber. The beam fiber elements adjacent to the column are used to model connection gap opening. The fibers of the beam cross section initially in contact with the shim plates are assigned a stress-strain relationship that has stiffness in compression, but none in tension. To properly account for the depth of the beam and the size of the panel zone in the connection region, it was necessary to utilize a set of master-slave nodes as shown in Fig. 5. The panel zone region is modeled by placing two rotational springs. The strands and friction dampers were modeled using truss elements and spring elements having a rigid-plastic force deformation relationship, respectively.

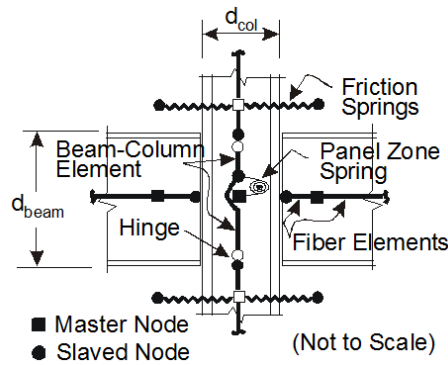


Figure 5. PT-FFD connection analysis model

A Drain-2DX model of the frame was created. The beams, columns, and panel zones were modeled using fiber elements and springs as described previously. P-delta effects from the building interior gravity frames were incorporated into the model using a leaning column. Gravity loads (unfactored) were applied to the MRF and the leaning column. The masses at each floor of the frame were located at the leaning column. The interaction between the floor diaphragm system and the SC-MRF was also modeled via springs that model the strength and the stiffness of four collector beam elements (see Figure 4(a)) which are connected to the columns of the SC-MRF. Additional details about the nonlinear analytical modeling of the frame can be found in Rojas (2003).

## 6. SEISMIC PERFORMANCE OF THE SC-MRF

### 6.1. Nonlinear Static Pushover Analysis

A nonlinear static pushover analysis of the frame was conducted with the aid of the DRAIN-2DX program. The lateral loads were distributed over the height of the frame in accordance with the ASCE/SEI 7-10 provisions. Figure 6 shows the relationship between the normalized base shear and the roof drift of the frame. The normalized base shear is the base shear divided by the seismic dead weight of the building,  $W$ , while the roof drift is the roof displacement divided by the overall height of the frame. On this plot, the onset of each limit state and the design relative rotation at the DBE and MCE levels are marked.

The first connection gap opening occurs at a base shear of  $0.029W$ , corresponding to a roof drift of

0.29%. The beginning of a significant reduction in the frame lateral stiffness occurs at a base shear of  $0.06W$  due to gap opening of several connections. First yielding occurs at the base of the ground floor columns when the applied base shear is  $0.075W$  and the roof drift is 1.63%. Beam compression yielding at the end of the reinforcing plates begins when the roof drift is 2.37%. First yielding of the panel zones and the collector beams begin when the roof drift are 2.88% and 3.46%, respectively.

The maximum overstrength of the frame is 2.49 ( $0.092W$ ) when the roof drift is 3.45% while the overstrength of the frame is 2.30 ( $0.085W$ ) when the roof drift is 5%. The DBE and MCE overstrengths are 2.38 ( $0.088W$ ) and 2.45 ( $0.091W$ ) corresponding to roof drifts of 2.68% and 4.02%, respectively. The maximum interstory drift was 6.39% and occurred at the second story. The maximum connection relative rotation,  $\theta_r$ , was 0.065 radians and occurred at the third bay of the first floor.

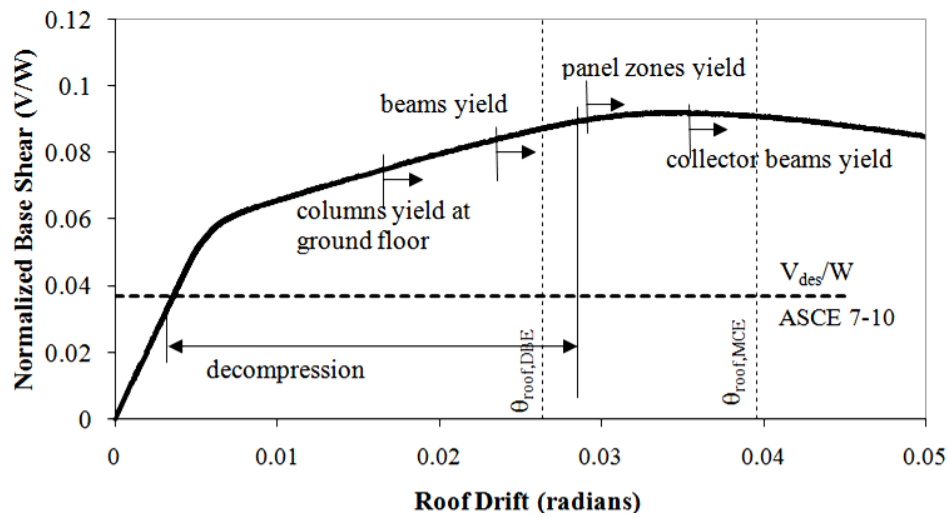


Figure 6. Static pushover results

## 6.2. Nonlinear Time History Analyses

Nonlinear dynamic time history analyses were conducted using an ensemble of four accelerograms to investigate the seismic behavior of the SC-MRF with PT-FFD connections. These accelerograms include two US records taken from the PEER (Pacific Earthquake Engineering Research Center) database and two Japanese records taken from the SAC database. These accelerograms were chosen since these records were the most demanding in the study of Rojas (2003) for the 4 bay six story SC-MRF. Two sets of analyses were conducted. For the first set of analyses, the four ground motions were scaled to the DBE level. For the second set, the four ground motions were scaled to the MCE level. The scaling procedure developed by Somerville (1997) was used, with the ASCE/SEI 7-10 DBE and MCE response spectra as the target spectra. The ASCE/SEI 2010 DBE and MCE response spectra are compared to the response spectra for the four DBE level scaled ground motions in Figure 7. The first and second modal periods ( $T_1$  and  $T_2$ ) are 2.65 and 0.98 seconds, respectively. It can be seen from Figure 7 that the Gilroy and the Canoga records have the largest spectral accelerations at  $T_1$  while the Kobe and the Miyagi have the largest spectral accelerations at  $T_2$ .

Table 6.1 presents a summary of the seismic response of the SC-MRF in terms of the maximum magnitude of roof drift ( $\theta_{\text{roof,max}}$ ), interstory drift ( $\theta_{\text{max}}$ ), residual interstory drift ( $\theta_{\text{res,max}}$ ), relative rotation ( $\theta_{r,\text{max}}$ ), and the base shear ( $V_{\text{max}}$ ) at the DBE and MCE levels. No statistical results are presented in the table since the research considers evaluating the seismic performance of the SC-MRF using an ensemble of eight accelerograms instead of the four chosen for this paper. This research is currently underway. It can be seen that the Kobe and the Miyagi records produce the largest values of story drifts, relative rotations, and base shears at both ground motion levels. The largest interstory drifts occurred at the upper stories for both ground motion levels for the Japanese records. This is due

to the fact that the connections located at the upper floors are weaker than those located at the lower floors. As a result, the upper floor connections develop larger relative rotation,  $\theta_r$ , with increasing ground motion intensity which produce larger interstory drifts. In addition to this, it is seen from Figure 7 that between periods of 0.75 and 1.5 seconds the Japanese records, scaled to the DBE level, have larger pseudo-accelerations than the ASCE/SEI 7-10 DBE and MCE response spectra. Therefore, it can be concluded that when softening behavior occurs in the SC-MRF (due to many connections experiencing gap opening) the second mode period elongates and affects the overall response of the frame.

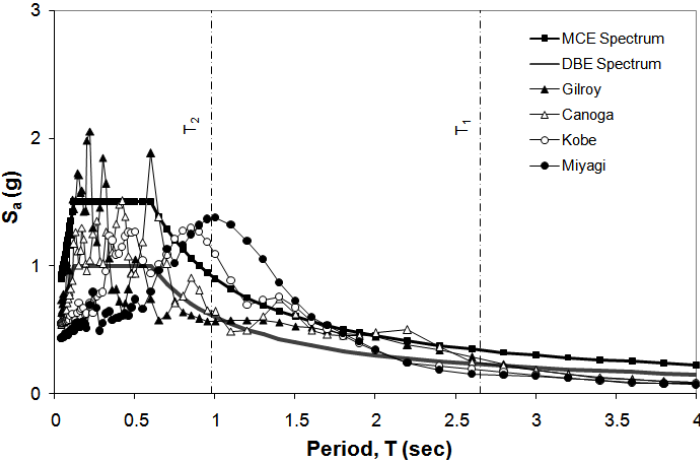


Figure 7. Response spectra

The maximum residual interstory drifts are in general negligible at the DBE and MCE level for the US records as seen in Table 6.1. However, the Miyagi ground motion at both levels produce the largest residual interstory drift (0.42% and 0.87%) which occurred at the first story. Nevertheless, these values can be considered satisfactory if one compares these quantities with the values indicated in Table 4-2 of FEMA 350 for the immediate occupancy (limited to 1%) and collapse prevention (large) levels. Figure 8 presents the mean ( $m$ ) and the mean plus one standard deviation ( $m+\sigma$ ) for the residual interstory drifts. It is seen that the residual interstory drifts are negligible at the DBE level while at the MCE level they are not quite negligible due to severity of the Japanese ground motions.

The roof time history displacement under the Gilroy and the Miyagi records at both ground motion levels is shown in Figure 9. It can be seen in Figure 9, that the MRF shows a reduced response and self centers for the Gilroy record under both ground motion levels while under the Miyagi DBE and MCE records shows a small residual floor displacement (38.6 and 127 mm, respectively).

The estimated values of 0.0274 and 0.0471 radians for connection relative rotation ( $\theta_r$ ) agrees reasonably well with the peak values of the Gilroy and Canoga records at the DBE and MCE levels as seen in Table 6.1. On the contrary, the estimated values for connection relative rotation ( $\theta_r$ ) underestimates the peak values of the Kobe and Miyagi records at the DBE and MCE levels as seen in Table 6.1. The peak values for the records usually occurred at either the roof or the seventh level. The  $M/M_{pn}$  – relative rotation response ( $\theta_r$ ) of the SC-MRF, subjected to the Miyagi and Gilroy DBE and MCE records, is plotted in Figure 10 at the central bay of the fifth floor-right side. On these plots, it is included the design curve. It is seen that the design curve agrees reasonably well with both ground motions at both ground motion levels. However, as already discussed above, the design curve for the upper stories, especially the last two floors, underestimates the cyclic response especially for the Japanese records.

The maximum story shears are shown in Table 6.1 at both ground motion levels. The mean DBE and MCE values are 12.2% and 14.8%W, respectively. If these mean values are divided by the design base shear (3.7%W according to ASCE/SEI 7-10), the “dynamic overstrength factors” at the DBE and

MCE levels result in 3.3 and 4.0, respectively. These values are significantly larger than the values obtained (2.38 and 2.45) from the nonlinear pushover analysis and the dynamic quantities reported in Rojas (2003) for the 6 four bay story SC-MRF.

**Table 6.1.** Response of SC-MRF with PT-FFD connections

Ground Motion	$\theta_{\text{roof,max}}$ (%)		$\theta_{\text{max}}$ (%)		$\theta_{\text{res,max}}$ (%)		$\theta_{r, \text{max}}$ (rads)		$V_{\text{max}}$ (%W)	
	DBE	MCE	DBE	MCE	DBE	MCE	DBE	MCE	DBE	MCE
Gilroy	1.79	2.44	3.23	4.80	0.035	0.043	0.0259	0.0416	9.4	12.2
Canoga	1.99	2.84	2.08	4.90	0.037	0.167	0.0267	0.044	11.9	13.7
Kobe	1.63	2.10	4.37	6.90	0.025	0.50	0.0386	0.067	13.0	17.1
Miyagi	2.05	3.33	5.65	6.87	0.42	0.87	0.0557	0.067	14.4	16.3

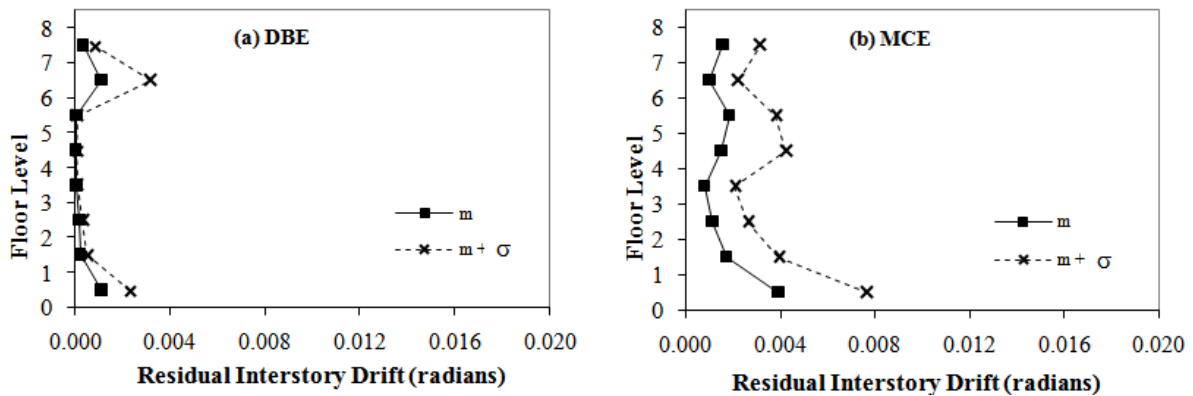


**Figure 8.** Residual Interstory drifts from nonlinear dynamic analyses for the DBE and MCE records

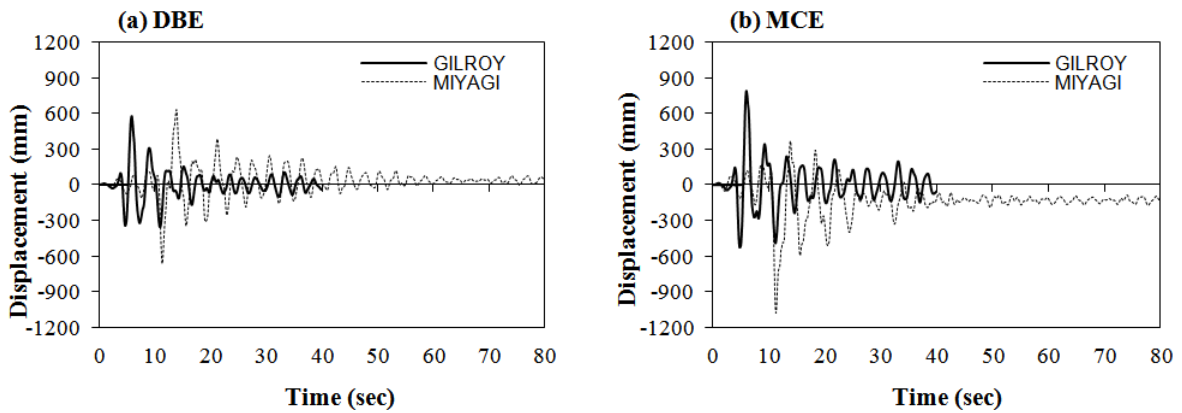


**Figure 9.** Roof displacement under the Gilroy and Miyagi records

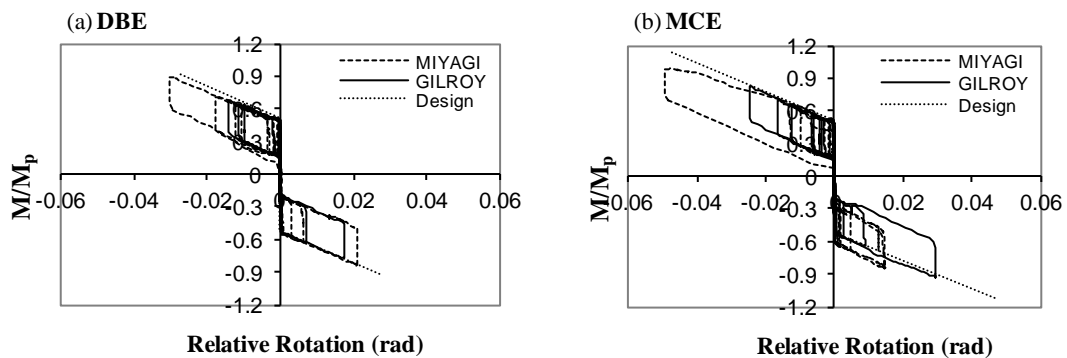


**Figure 10.** Connection behavior under the Gilroy and the Miyagi records; Central Bay of fifth floor- right side

## 7. SUMMARY AND CONCLUSIONS

The seismic evaluation of a SC-MRF with PT-FFD beam-to-column connections has been presented. The eight story MRF has three-25 feet bays. The frame was designed using a performance based design procedure and according to the ASCE/SEI 7-10 seismic provisions using a modal response spectrum analysis. Nonlinear static pushover and dynamic time history analyses were carried out. Four ground motions, scaled at the DBE and MCE levels were used. Results of the analyses show that the seismic performance of the SC-MRF with PT-FFD connections has adequate strength, ductility, energy dissipation, and especially self-centering capabilities. Under DBE and MCE ground motions, the SC-MRF was able to comply with the design performance objectives. Future work shall address better estimates of connection relative rotation under records such as the Japanese records and taller frames than the ones studied by the authors.

## ACKNOWLEDGEMENTS

This research is based upon work to be presented to the Civil Engineering Department of the Escuela Superior Politécnica del Litoral (ESPOL) of Guayaquil-Ecuador in candidacy for the degree of Civil Engineer of Miss Diana C. Suárez. The research reported herein was done with the participation of the ESPOL and Lehigh University. The authors are grateful to Dr. María Garlock and Gordana Herning from Princeton University for their valuable comments to this research. The findings, opinions, and conclusions expressed in this paper are the authors' and do not necessarily reflect the opinions of those acknowledged here.

## REFERENCES

- American Society of Civil Engineers, (2010). Minimum Design Loads for Building and Other Structures. ASCE/SEI 7-10. Reston VA, 608 p.
- Caballero, M. (2005). Rehabilitación Sísmica de Pórticos de Acero Resistentes a Momento con Conexiones Postensadas y Elementos de Fricción. Tesis de Grado, Facultad de Ingeniería en Ciencias de la Tierra, Escuela Superior Politécnica del Litoral, Guayaquil-Ecuador.
- FEMA (2003). NEHRP Recommended Provisions for Seismic Regulations for New Buildings and Other Structures. Part 1-Provisions and Part 2-Commentary, FEMA 450, Federal Emergency Management Agency, Washington D.C.
- Habibullah, A. and Wilson, E. (2009). SAP 2000: *Static and Dynamic Finite Element Analysis of Structures*, Advanced version 14.0. Computers and Structures, Inc., Berkeley, CA.
- Herrera, R., Sause, R., and Ricles, J. (2001). Refined Connection Element (Type 05) for DRAIN-2DX, Element Description and User Guide, *ATLSS Report No. 01-07*.
- Iyama, J., Seo, C-Y., Ricles, J.M., and Sause, R. (2008). Self-Centering MRFs with Bottom Flange Friction Devices under Earthquake Loading. *Journal of Constructional Steel Research*, pp.314-325.
- Lin, Y.C, Ricles, J.M. and Sause, R. (2008). Earthquake Simulations On A Self-Centering Steel Moment Resisting Frame with Web Friction Devices. *Proceedings, 14th World Conference on Earthquake Engineering*, Beijing, China.
- Prakash, V., Powell, G., and Campbell, S. (1993). DRAIN-2DX Base Program Description and User Guide, Version 1.0, *Report No. UCB/SEMM-93/17 & 18*. Structural Engineering Mechanics and Materials, Department of Civil Engineering, University of California, Berkeley, CA, December.
- Rojas, P. (2003). Seismic Analysis, Design, and Evaluation of Post-Tensioned Friction Damped Connections for Steel Moment Resisting Frames. Ph.D. Dissertation, Civil and Environmental Engineering Dept., Lehigh University, Bethlehem, PA.
- SAC (2000). Recommended Seismic Design Criteria for New Steel Moment-Frame Buildings. FEMA 350, prepared by the SAC Joint Venture for the Federal Emergency Management Agency (FEMA), Washington D.C.
- Somerville, P. (1997). Development of Ground Motion Time Histories for Phase 2 of the FEMA/SAC Steel Project. *Report No. SAC/BD-97/04*.
- Wolski, M., Ricles, J.M., and Sause, R. (2006). Seismic Resistant Self-Centering Steel Moment Resisting Frames With Bottom Flange Friction Devices. *Proceedings, 5th International Conference on Behavior of Steel Structures in Seismic Areas – STESSA 2006 Proceedings, Yokohama, Japan*.